J. of Supercritical Fluids 62 (2012) 165–172

Contents lists available at SciVerse ScienceDirect

The Journal of Supercritical Fluids

journal homepage: www.elsevier.com/locate/supflu

Investigation of counter-current mixing in a continuous hydrothermal flow reactor

Christopher J. Tighe[a,*], Robert I. Gruar[a], Cai Y. Ma[b], Tariq Mahmud[b], Xue Z. Wang[b], Jawwad A. Darr[a]

[a] Department of Chemistry, University College London, Christopher Ingold Laboratories, 20 Gordon Street, London WC1H 0AJ, UK
[b] Institute of Particle Science and Engineering, School of Process, Environmental and Materials Engineering, University of Leeds, Leeds LS2 9JT, UK

ARTICLE INFO

Article history:
Received 26 August 2011
Received in revised form
23 November 2011
Accepted 25 November 2011

Keywords:
Supercritical water jet
Hydrothermal synthesis
Nanoparticles
Counter-current mixing
Temperature profiles

ABSTRACT

Temperature profiles have been measured inside a counter-current mixer for the continuous hydrothermal synthesis of inorganic nanoparticles, at conditions (10–25 ml min^{-1} superheated water, referred to a density of 1 g ml^{-1}, at 350–450 °C and 24.1 MPa, mixed with precursors at 10–20 ml min^{-1}) used in work published by some of the authors and others. The superheated water cooled significantly before meeting the precursors, owing to internal transfer of heat through the wall of the inner tube to the products flowing around it. Consequently, the region immediately after the fluids had fully mixed was at a lower temperature than that determined from an overall heat balance. The flow of superheated water emerging from the inner pipe was characterised using the relevant dimensionless groups (Reynolds, Froude).

1. Introduction

1.1. Continuous hydrothermal synthesis of nanoparticles

The production of inorganic nanoparticles (particles with a length scale typically between 1 and 100 nm) by continuous hydrothermal processes [1–3] is attracting widespread interest. The nanoparticles, which are typically oxides of metals, have many potential applications, *e.g.* as catalysts [4], photocatalysts [5], bioceramics [6] and in components of solid oxide fuel cells [7]. In our process, here termed continuous hydrothermal flow synthesis (CHFS), superheated water (typically above the critical point of water, T_c = 374 °C and P_c = 22.1 MPa) is mixed with water soluble precursors, such as the nitrate of a metal, in aqueous solution at ambient temperature; upon mixing, the precursors are heated rapidly so that the metal salt undergoes a fast reaction to form a slurry containing metal oxide nanoparticles.

1.2. Mixers for CHFS

The method by which the superheated water is contacted with the solution of metal salt can influence properties of the nanoparticles (*e.g.* size distribution) and the reproducibility of their synthesis [8]. Consequently, this field of literature is peppered with descriptions of many types of mixers, including tee-pieces [1], cross-pieces [9], and vortex-inducing devices [10]. One form [8] of counter-current mixer consisted of an inner pipe from which the superheated water emerged downwards, into an outer pipe through which the precursors flowed upwards; the reacting mixture subsequently travelled upwards through the annulus between the two pipes, towards the outlet. A similar counter-current device has been employed successfully for several years in research conducted by some of the authors, *e.g.* [4–7,11]; however, there is uncertainty in defining the 'true' reaction conditions in the mixer due to the arrangement of flows within this device.

The study of forced plumes is of particular relevance to this problem; however, the large body of academic literature in this field is mainly concerned with the release of a flow of a warm fluid into a slightly cooler, unconfined and stagnant environment [12]. Usually, the purpose is to predict the behaviour of discharges of flue gases from chimney stacks or warm aqueous waste outflows from factories into large bodies of water. Studies (*e.g.* [13]) of hydrothermal vents on the ocean flow are probably the closest analogue to mixing in the CHFS process. However, the counter-current mixer defies direct comparison to even this because: (i) the flow of superheated water is inverted, (ii) it issues into a counter-flowing environment confined by the outer tube, (iii) it is non-Boussinesq, *i.e.* there is significant difference in density between the superheated water and the cooler mixture flowing around it (a Boussinesq flow would be identical to that of a jet flowing vertically upwards with the identities of the fluids reversed), (iv) changes in transport and thermochemical properties of water with temperature are significant

* Corresponding author. Tel.: +44 20 7679 4312; fax: +44 20 7679 7463.
E-mail address: c.tighe@ucl.ac.uk (C.J. Tighe).

0896-8446/$ – see front matter © 2011 Elsevier B.V. All rights reserved.
doi:10.1016/j.supflu.2011.11.027

Nomenclature

A_o	outside surface area of inner pipe (m^2)
Fr	Froude number, given by Eq. (7)
G	mass flowrate ($kg\,s^{-1}$)
h	specific enthalpy ($kJ\,kg^{-1}$)
Q	volumetric flowrate ($ml\,min^{-1}$)
ΔQ	rate of heat transfer (W)
Re	Reynolds number, given by Eq. (6)
T	measured temperature (°C)
T'	temperature calculated by heat balance (°C)
ΔT_{lm}	log-mean temperature difference (K)
U_o	overall heat transfer coefficient based on A_o ($W\,m^{-2}\,K^{-1}$)
z	distance from outlet of superheated water (mm)

Greek symbols

μ	viscosity (Pa s)
θ	temperature difference (K)
ρ	density ($kg\,m^{-3}$)

Subscripts

hw	superheated water
in	inlet to mixer
m	mixture of superheated water and 'precursors'
out	outlet of mixer
p	'precursors' (de-ionised water)

near the critical point [14], *e.g.* resulting in rapid thermal dilation of the jet as it cools and (v) the temperature gradient is very large in the region around the exit of the inner tube, so the conduction of heat is probably important and temperature may not be a passive scalar. Attempts have been made [8] to visualise the behaviour of a tracer in such systems, using transparent plastic mock-ups at ambient temperature and pressure; however, application of the results of such models to a CHFS process at a working temperature and pressure must be approached with caution, because the effects of (iv) and (v) above in particular are neglected.

Novel experimental methods have been used to visualise certain properties of a hydrothermal system at working temperatures and pressures. The distribution of nanoparticles of ceria within a counter-current mixer operating at 450 °C and 24.1 MPa was mapped in situ using X-rays from a synchrotron [15]. This showed a plume issuing from the inner pipe and rising upwards, in or around which the ceria formed; analysis of the Bragg peaks using the Scherrer equation provided evidence of the initial nucleation and subsequent growth of the nanoparticles as they travelled towards the outlet. Schlieren photography through a sapphire window has recently been used [16] to visualise a jet of supercritical water (22.3 MPa, up to 500 °C and a flowrate of $4\,g\,s^{-1}$) emerging from a nozzle (diameter 1–4 mm) into a body of water at ambient temperature. In most of the experiments, it was found that the flow did not remain supercritical beyond a length equivalent to one nozzle diameter, due to entrainment of the surrounding ambient water.

Computational fluid dynamic (CFD) simulations may be used [17,18] to visualise the processes of momentum, heat and mass transfer occurring inside a counter-current mixer. Such simulations are not trivial, because the transport properties of water change markedly around the critical point [14]. Mixing has been simulated [18] in a counter-current reactor, under three conditions: natural and forced convection of the superheated water, and a balance between the two. For natural convection, the mixing of the superheated water and precursors occurred in the immediate vicinity of the outlet (well within a length equivalent to one diameter of the inner pipe). In the case of forced convection of the superheated water, the mixing zone extended much further (~4 diameters) into the precursors; however, the associated temperature and velocity fields were not reported with these results. Despite this prior work, the environment within a counter-current mixer remains poorly defined.

The objective of this study was to gain a deeper understanding of the transport processes occurring inside the counter-current mixer. To achieve this, detailed measurements of temperature profiles were made, using fine thermocouples inserted into the flow under conditions (10–25 ml min^{-1} superheated water, referred to a density of 1 g ml^{-1}, at 350–450 °C and 24.1 MPa, mixed with precursors at 10–20 ml min^{-1}) relevant to the continuous hydrothermal synthesis of nanoparticles. This work builds in particular on a measurement of the temperature profile in a counter-current mixer [19] at a much lower temperature.

2. Materials and methods

2.1. Apparatus for continuous hydrothermal flow synthesis

Fig. 1 shows a flow diagram of the CHFS apparatus. Pump P1 (Gilson HPLC) was used to pump deionised (DI) water at 24.1 MPa and a flowrate of between 10 and 25 ml min^{-1} (referred to a density of 1 g ml^{-1}). The time taken for this positive displacement pump to complete one stroke (discharge and refill) was 125 ms. The water flowed upwards through a 6 m length of tubing (316 stainless steel, 6.35 mm outside diameter) coiled around an aluminium rod. The rod was electrically heated (up to 2.5 kW) and the heater assembly was insulated (Thermal Ceramics Superwool 607 blanket, thickness 5 mm). The temperature of the aluminium rod, measured by a thermocouple (type J, 316 stainless steel sheath, 3 mm) embedded in the top, was held constant between 350 and 450 °C. The superheated water exiting the coil was assumed to be in thermal equilibrium with the aluminium rod.

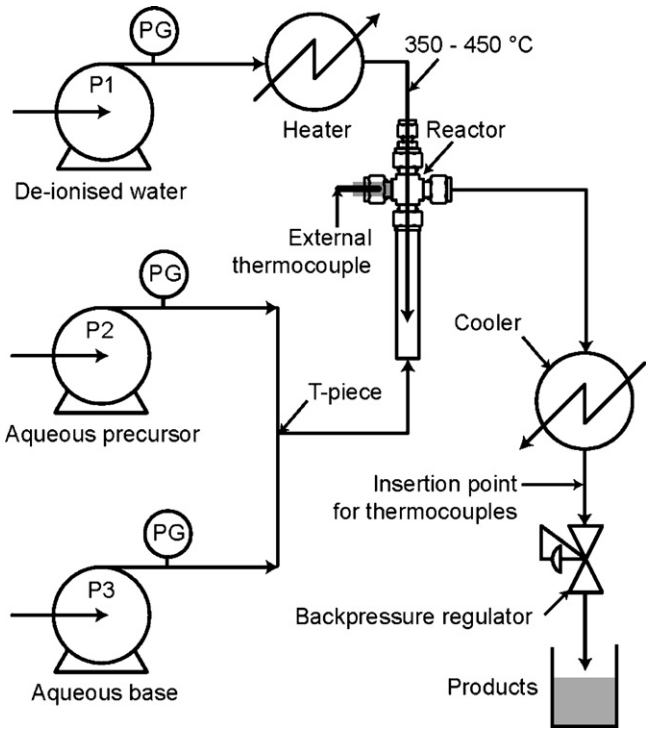

Fig. 1. Flow diagram showing the continuous hydrothermal flow synthesis apparatus used in this study (P1–P3: HPLC pumps, PG: pressure gauge). For the in situ temperature measurements all the flows were DI water.

In the production of nanoparticles, P2 and P3 (identical to P1) pump precursors at room temperature and a flowrate of between 5 and 10 ml min^{-1} from each pump. However, for this study, P2 and P3 pumped only DI water as it was found that synthesising nanoparticles with the thermocouples in place caused a blockage to form after only a few minutes. In order to aid its distinction from the superheated water, the combined flow from P2 and P3 will henceforth be referred to as 'precursors'.

The 'precursors' were mixed with the superheated water using the counter-current arrangement shown in Fig. 2. The mixer was constructed from compression fittings (316 stainless steel, fractional sizes, Swagelok) and the corresponding instrument tubing (316 stainless steel). The inner tube (3.18 mm OD tube, 0.71 mm wall thickness), through which the superheated water flowed downwards, entered the topmost port of a 3/8" cross-piece via an adaptor; this was modified to allow the tubing to be inserted completely through it, such that the end of the inner tube terminated 72 mm below a horizontal line drawn through the centre of the cross-piece. A larger section of tube (9.53 mm OD, wall thickness 1.24 mm, length 100 mm) was inserted over the inner tube and into the lower port of the cross piece; the 'precursors' flowed upwards through this tube where it met with the superheated water. A metal block (316 stainless steel, 9.53 mm OD) drilled out to allow the insertion of a thermocouple (type J, 316 stainless steel sheath, 3 mm OD) was inserted into one of the side ports of the cross-piece. The tip of the thermocouple lay ~ 2 mm short of the pressurised chamber within the cross-piece. This measurement has been reported in previous work as the reaction temperature when producing nanoparticles [20–23]. The entire assembly was insulated from the outlet from the heater to the inlet to the cooler.

The products exited the mixer through a tube (9.53 mm OD, wall thickness 1.24 mm) inserted into the remaining side port and were cooled using a heat exchanger, the design of which has been described in detail elsewhere [14]. The pressure in the system was maintained constant at 24.1 MPa using a back-pressure regulator (BPR) positioned at the outlet of the cooler.

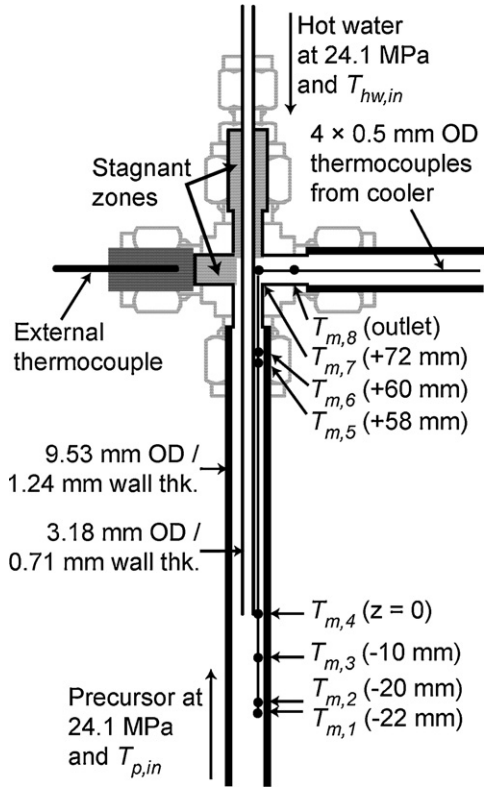

Fig. 2. Details of the counter-current reactor showing the locations of the thermocouples during the in situ measurements of temperature.

2.2. In situ measurements of temperature

Temperature profiles were measured inside the counter-current mixer by inserting four fine thermocouples (type J, stainless steel sheath, 0.5 mm OD, 1.0 m length) into the apparatus, between the cooler and the BPR as indicated in Fig. 1, each of which terminated at a different position (shown in Fig. 2). The temperature at eight different locations in the mixer was measured in two separate runs. The cross-sectional area of the four thermocouples combined was 0.8 mm^2, compared the cross-sectional area of 36.6 mm^2 of the annulus formed between the inner and outer pipe of the mixer. Thus, the thermocouples occupied only ~2% of the cross-sectional area of the annulus. The tips of the thermocouples were not fixed to a surface and were angled such that they would protrude into the flow during an experiment. This permitted the temperature to be measured in the bulk flow; however, this also meant that slight radial movement of the tip may occur in the flow, thus, the positions of the thermocouples are quoted to ca. ±2 mm since the stiffness in the thermocouples inhibited their movement to some degree. The response time of the thermocouples (the time taken to reach 63.2% of the temperature steady-state when plunged into a batch of boiling water) was quoted by the manufacturers as ~25 ms. The temperature at each location was recorded every 500 ms.

3. Results and discussion

3.1. Measurements of temperature with time

Fig. 3 shows a typical sample of the four simultaneous measurements of temperature at the locations in the counter-current mixer corresponding to $z = 0$, −10, −20 and −22 mm in Fig. 2. At a time, $t = 0$ in Fig. 3, the flowrates of superheated water, Q_{hw}, and 'precursors', Q_p, were each 20 ml min^{-1}. Henceforth, this is referred to as 'balanced flows', *i.e.* the opposing flows of superheated water and precursors are equal on a mass basis (in reality, the volumetric flowrate of the superheated water greatly exceeded that of the 'precursors' owing to the difference in densities). At $t = 150$ s, the flowrate of superheated water was increased to 25 ml min^{-1} and the flowrate of 'precursors' was reduced to 10 ml min^{-1}; this condition is referred to hereafter as 'unbalanced'.

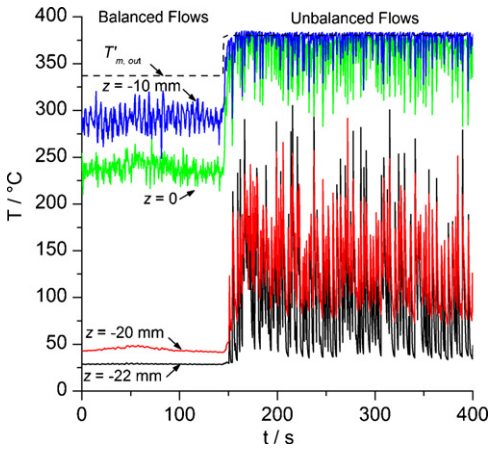

Fig. 3. Measurements of temperature against time during a transition between balanced flowrates ($Q_{hw} = Q_p = 20$ ml min^{-1}) and unbalanced flowrates ($Q_{hw} = 25$ ml min^{-1}, $Q_p = 10$ ml min^{-1}). Here, $T_{p,in} = 20$ °C, $T_{hw,in} = 450$ °C and the dashed line, labeled $T'_{m,out}$, is the maximum theoretical temperature at the outlet of the mixer determined from Eq. (1).

The noisy measurements seen in the right hand side of Fig. 3 are not the result of electrical or other interference in the measurement system. However, the response time of the thermocouples (~25 ms) and the sampling rate (500 ms) were most likely too slow to capture temperature fluctuations arising from turbulence, which are typically on a time scale of a only a few milliseconds. The fluctuations may have resulted from inhomogeneities in the fluids due to the time taken for the positive displacement HPLC pumps to refill (125 ms). Alternatively, small movements in the tips of the thermocouples, exacerbated by large temperature gradients around the mixing point, may have been responsible for the fluctuations. This also made it difficult to assess the extent to which the presence of the thermocouples disturbed the flow in the mixing zone below the outlet of the inner tube (*i.e.* by removing all but one of the thermocouples) because it was impossible to ensure the tip of a thermocouple was in the same place as a previous experiment (*e.g.* at $z = 0$ with the three thermocouples at negative z removed) resulting in a significant change from the previously measured temperature.

When the flows were balanced, at a distance of >20 mm below the inlet of the superheated water, the measured temperature was approximately equal to the inlet temperature of the 'precursors', $T_{p,in} = 20\,^{\circ}C$. This proves that, at these balanced flowrates, the superheated water issuing from the inner tube does not penetrate this far into the 'precursors'. Interestingly, Fig. 3 also shows that the temperature measured at $z = 0$ mm was significantly cooler than at $z = -10$ mm, whereas it would be expected to be hotter. The thermocouple at $z = 0$ was located to one side of the mouth of the inner tube (as shown in Fig. 2) not directly below it, so the fluid flowing past the tip of the thermocouple should be a mixture of superheated water and 'precursors'. Assuming the downward flow of superheated water turned upwards immediately after emerging from the inner pipe, the thermocouple located at $z = -10$ mm would be in a flow of 'precursors'. Thus, this observation suggests that either there was significant conduction of heat against the flow of 'precursors', or that the thermocouple located at $z = -10$ mm was in fact protruding into the boundary between the 'precursors' and a jet or plume of superheated water issuing from the inner pipe, which had not fully mixed with the 'precursors'. When the flows were unbalanced (after $t = 150$ s, in Fig. 3) temperature measurements at or below $z = -20$ mm indicate penetration of the superheated water deep into the flow of 'precursors' and a very high degree of instability (*i.e.* noise) in the temperature measurements at all the thermocouple locations.

The dashed line in Fig. 3 shows the maximum theoretical temperature calculated for the outlet of the mixer (*i.e.* the inlet to the cooler) assuming mixing is complete and any heat losses from the outer pipe to the surroundings are negligible. This was determined from the overall enthalpy balance:

$$h_{m,out}\ (T'_{m,out},\ 24.1\,\text{MPa}) = \frac{G_{hw} h_{hw,in}(T_{hw,in},\ 24.1\,\text{MPa}) + G_p h_{p,in}(T_{p,in},\ 24.1\,\text{MPa})}{G_{hw} + G_p}, \quad (1)$$

where G_{hw} and G_p are the mass flow rates of the superheated water and 'precursors', respectively. The specific enthalpies $h_{hw,in}$ and $h_{p,in}$ and the temperature, $T'_{m,out}$, at which the specific enthalpy is $h_{m,out}$ at 24.1 MPa were determined from the IAPWS Formulation 1995 for the Thermodynamic Properties of Ordinary Water Substance for General and Scientific Use [24] using the associated FLUIDCAL software. This software was also used to calculate the density and viscosity of water for any given temperature at 24.1 MPa.

It can be seen in Fig. 3 that when the flow rates of the precursor and superheated water were balanced, the 30 second time-averaged temperature at $z = 0$ was ~100 °C lower than the expected theoretical outlet temperature for this location. In fact, it shall be shown later that, assuming the 'precursors' and superheated water are fully mixed at $z = 0$, this apparent discrepancy was due in part to the conduction of heat from the superheated water flowing downwards through the inner tube to the cooler products flowing upwards through the annulus between the inner and outer tubes. Thus, the temperature of the superheated water exiting the inner tube was considerably lower than $T_{hw,in}$. When the flowrates were unbalanced, the maximum temperature at both $z = 0$ and -10 mm was equal to $T'_{m,out}$, suggesting violent mixing in the region around the exit of the inner tube; however, the temperatures measured inside the mixer were highly unstable under these conditions, which may be considered undesirable for the controlled synthesis of nanoparticles.

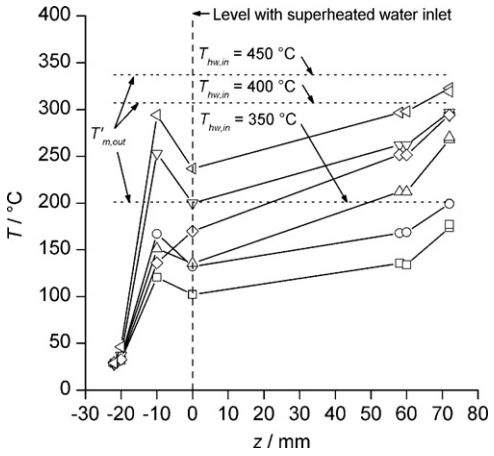

Fig. 4. Temperature profiles in the balanced flow regime ($T_{p,in} = 20\,^{\circ}C$ for all experiments; □ $T_{hw,in} = 350\,^{\circ}C$, $Q_{hw} = Q_p = 10$ ml min^{-1}; ○ 350 °C, 20 ml min^{-1}; △ 400 °C, 10 ml min^{-1}; ◊ 400 °C, 20 ml min^{-1}; ▽ 450 °C, 10 ml min^{-1}; ◁ 450 °C, 20 ml min^{-1}).

3.2. Time-averaged temperature profiles at $z \leq 0$

Figs. 4 and 5 are plots of the mean temperatures (averaged over 30 s) measured inside the counter-current mixer for balanced and unbalanced flowrates, respectively. In all except one of the experiments, the temperature at $z = -10$ mm was higher than that at $z = 0$. Thus, as before, it appears the thermocouple at $z = -10$ mm was protruding into a jet or plume of superheated water issuing from the inner tube. The exception was the plot at $T_{hw,in} = 400\,^{\circ}C$ and $Q_{hw} = Q_p = 20$ ml min^{-1} in Fig. 4. Here, the temperature increased

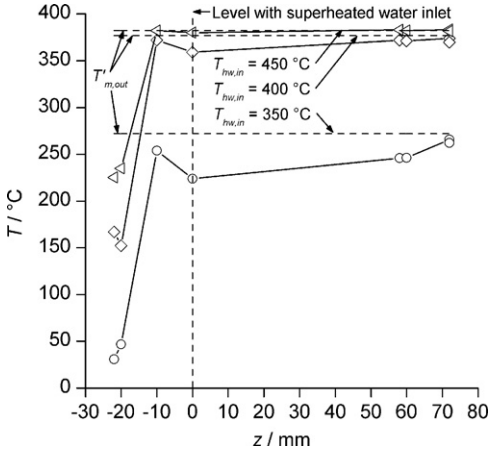

Fig. 5. Temperature profiles in the unbalanced flow regime ($T_{p,in} = 20\,^{\circ}C$, $Q_{hw} = 25$ ml min^{-1} and $Q_p = 10$ ml min^{-1} for all experiments; ○ $T_{hw,in} = 350\,^{\circ}C$; ◊ 400 °C; ◁ 450 °C).

monotonically with z. This effect was probably due to a small, temporary deviation in the tip of the thermocouple at $z = -10$ mm, away from the jet of superheated water. The temperature profiles in Fig. 4 show that, at a distance of 20 mm below the inlet of the superheated water, the temperature in the flowing precursor feed was approximately equal to $T_{p,in}$, irrespective of $T_{hw,in}$. Thus, when the flowrates of the 'precursors' and superheated water feeds were balanced, the superheated water issuing from the inner tube never penetrated far into the oncoming 'precursors'. Conversely, when the flowrates were unbalanced, it is evident from Fig. 5 that very high temperatures (which were also highly unstable as in Fig. 3) were measured at a distance of 20 mm below the inlet of the superheated water. Interestingly, for the unbalanced flows, the temperature measured at $z = -20$ mm increased significantly with increasing $T_{hw,in}$, suggesting that the depth of penetration of the jet or plume of supercritical water increased with $T_{hw,in}$.

3.3. Time-averaged temperature profiles at $z \geq 0$

Attention is turned next to the temperatures profiles measured at $z \geq 0$, in the annulus between the inner and outer tubes. For balanced flowrates (Fig. 4), the temperature of the fluid moving up through the annulus increased; this was the result of the conduction of heat from the hotter superheated water, flowing downwards through the inner tube. Consequently, the temperature of the superheated water issuing from the inner pipe was in fact less than $T_{hw,in}$. This internal transfer of heat was also evident to a lesser extent in Fig. 5 and will be addressed next; however, it can be disregarded for the purpose of comparing the temperature measured at the outlet of the mixer to $T'_{m,out}$, determined from Eq. (1) assuming mixing was complete and heat losses were negligible. Values of $T'_{m,out}$ determined for each experiment are given in Table 1, along with the temperature measured at $z = 72$ mm for comparison (the reading on this thermocouple was always the same as the one positioned in the outlet from the mixer in Fig. 2). The external thermocouple (also shown in Fig. 2) typically read ~20 °C lower than the thermocouple at $z = 72$ mm at steady-state. For balanced flowrates with $Q_{hw} = Q_p = 10$ ml min^{-1}, the difference between the temperature measured at the outlet and $T'_{m,out}$ was between 27 °C (run 1 in Table 1) and 43 °C (run 7). When both flowrates were increased to 20 ml min^{-1}, the discrepancy was found to be between 1 °C (run 2) and 14 °C (run 8). For the experiments using unbalanced flows (shown in Fig. 5), the temperature measured at the outlet of the mixer was the same as $T'_{m,out}$, which suggests that the assumptions of Eq. (1) hold at these conditions.

3.4. Internal heat transfer

It is apparent from the temperature profiles in Figs. 4 and 5 that the mixture flowing through the annulus ($z \geq 0$), assumed to be completely mixed, was not isothermal. This would be of concern to the experimentalist, because the reaction conditions vary considerably over the region where nanoparticles nucleate and grow. Furthermore, the temperature of the superheated water in the region where it met with the 'precursors' (in the region of $z = 0$) was in fact lower than the temperature at which it entered the mixer, $T_{hw,in}$. This drop in temperature will now be quantified.

The transfer of heat between the superheated water inside the inner tube to the cooler mixer flowing through the annulus between the inner and outer tubes is akin to a simple countercurrent, pipe-in-pipe heat exchanger. The heat lost from the superheated water, $-\Delta Q_{hw}$, must be equal to the heat gained by the cooler mixture, ΔQ_m, determined by the enthalpy balance:

$$\begin{aligned}\Delta Q_m &= -\Delta Q_{hw} \\ &= (G_{hw} + G_p)[h_{m,z=72}(T_{m,z=72},\ 24.1\,\text{MPa}) \\ &\quad - h_{m,z=0}(T_{m,z=0}, 24.1\,\text{MPa})],\end{aligned} \tag{2}$$

The specific enthalpy and thus the temperature of the superheated water exiting the inner tube at $z = 0$ may subsequently be determined from:

$$\begin{aligned}&h_{hw,z=0}(T'_{hw,z=0}, 24.1\,\text{MPa}) \\ &\quad = h_{hw,in}(T_{hw,in}, 24.1\ \text{MPa}) + \Delta Q_{hw}/G_{hw}.\end{aligned} \tag{3}$$

Values of $T'_{hw,z=0}$ determined from Eqs. (2) and (3) are given in Table 1. This was not calculated for the unbalanced flows at $T_{hw,in} = 400$ and 450 °C because, although the temperature rise from $z = 0$ to 72 mm was only a few Kelvin, the magnitude of ΔQ_m from Eq. (2) was very large owing to the dramatic increase in the specific heat capacity of water near to its critical temperature. Consequently, the magnitude of ΔQ_{hw} and thus $T_{hw,z=0}$ were very sensitive to any errors in the temperature measurements for these two experiments. The large quantity of heat, calculated to be lost from the superheated water flowing down through the inner pipe, was striking: up to 0.3 kW at the highest flowrates (runs 5 and 8 in Table 1), equivalent to a heat flux of 417 kW m^{-2} averaged over the outer surface area of the inner tube, A_o ($= 7.2 \times 10^{-4}$ m^2). This is approximately one third of the power used to heat the water from 20 to 450 °C. Thus, the temperature of the superheated water exiting the inner pipe could be significantly lower than that entering the mixer from the heater, even after considering heat losses from the pipes evident from the difference between $T_{m,z=72}$ and $T'_{m,out}$ in Table 1.

The magnitude of ΔQ_m depends on the overall heat transfer coefficient, U_o, of the 'heat exchanger'. Without the temperature measurements from this work, U_o cannot be reliably estimated in the usual manner (from Nusselt number correlations involving

Table 1
Temperature profiles (30-s time averaged) in countercurrent mixer at various precursor and superheated water flowrates ($T_{p,in} = 20$ °C for all experiments). $T'_{m,out}$ is the outlet temperature calculated from Eq. (1). $T_{hw,z=0}$ was the temperature of the superheated water leaving the inner pipe calculated from Eq. (2). $\text{Re}_{hw,z=0}$ and $(\text{Fr}_{hw,z=0})^2$ are the dimensionless Reynolds and Froude numbers for the jet of superheated water at $z = 0$.

No.	$T_{hw,in}$ (°C)	Q_{hw} (ml min^{-1})	Q_p (°C)	$T_{m,z=0}$ (°C)	$T_{m,z=72}$ (°C)	$T'_{m,out}$ (°C)	$T'_{hw,z=0}$ (°C)	U_o (W m^{-2} K^{-1})	$\text{Re}_{hw,z=0} \times 10^3$	$(\text{Fr}_{hw,z=0})^2$
1	350	10	10	102	174	201	236	907	1.0	2.5
2	350	20	20	132	200	201	242	2059	2.1	11.5
3	350	25	10	224	266	272	305	1878	3.4	19.3
4	400	10	10	135	268	307	323	1703	1.5	1.6
5	400	20	20	200	297	307	362	3203	3.6	6.2
6	400	25	10	359	374	377	–	–	9.8	21.8
7	450	10	10	170	294	337	373	1467	2.1	1.3
8	450	20	20	237	323	337	381	2907	5.9	6.5
9	450	25	10	380	383	382	–	–	10.5	44.9

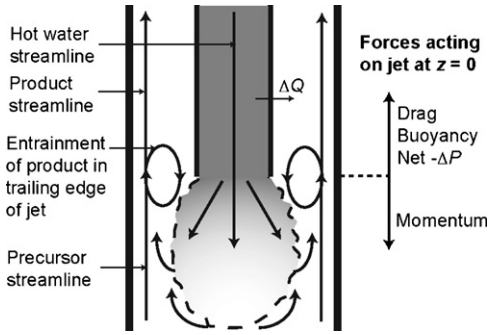

Fig. 6. Simplified representation of the momentum and heat transfer processes and the forces acting on the jet of superheated water at $z = 0$.

the Reynolds and Prandtl numbers) owing to significant changes in transport and thermodynamic properties of water (*e.g.* density, viscosity, thermal conductivity and specific heat capacity) particularly when close to the critical temperature. However, U_o may be determined empirically from these experiments using:

$$U_o = \frac{\Delta Q_m}{A_o\ \Delta T_{lm}}, \tag{4}$$

where A_o ($= 7.2 \times 10^{-4}\ m^2$) is the outer surface area of the inner tube and ΔT_{lm} is the logarithmic mean temperature difference [25] given by:

$$\Delta T_{lm} = \frac{\theta_h - \theta_c}{\ln(\theta_h/\theta_c)},$$
$$\text{where } \theta_h = (T_{hw,in} - T_{m,z=72}) \text{ and } \theta_c = (T'_{hw,z=0} - T_{m,z=0}). \tag{5}$$

Table 1 gives the values of U_o determined from Eq. (4) for each of the experiments (except the two experiments using unbalanced flows at $T_{hw,in} = 400$ and 450 °C for the reasons given earlier). The magnitude of U_o was calculated to be between 908 and 3208 $W\,m^{-2}\,K^{-1}$, increasing as would be expected, with both increasing flowrate of superheated water downwards through the inner tube and flowrate of the mixture upwards through the annulus. The values of U_o in Table 1 are typical [25] for water-to-water heater transfer (900–1700 $W\,m^{-2}\,K^{-1}$) and heating of water using steam (1500–4000 $W\,m^{-2}\,K^{-1}$) and are consistent with previous measurements of U_o derived from temperature measurements within the cooler [14]. The higher values of U_o may be the result of enhanced heat transfer, which has been observed close to the critical point at low heat fluxes [26].

3.5. Forces acting on superheated water

It is interesting to consider the processes of momentum and heat transfer underpinning the counter-current mixer, in light of the temperature profiles measured in this work. As the superheated water exits the inner tube, the momentum of the jet is largely opposed by three forces: (i) drag due to the difference in velocity between the downward moving superheated water and the upward moving mixture, (ii) buoyancy due to differences in density and (iii) the net pressure gradient $-\Delta P/dz$ (*i.e.* the net flow must inevitably be upwards towards the outlet). Furthermore, it is well known [12] that jets entrain fluid in their wake, suggesting that in a counter-current geometry the mixture flowing upwards past the jet (containing nanoparticles under reaction conditions) may under some flow regimes be pulled back into the jet, resulting in re-circulation and a broadening of the residence time distribution of the mixer. Fig. 6 shows one simplified representation of the region immediately surrounding the exit of the inner tube.

The relative magnitude of the momentum of the jet of superheated water at $z = 0$ compared to the viscous drag force can be represented [27] by the Reynolds number, $Re_{hw,z=0}$, of the jet:

$$Re_{hw,z=0} = \frac{\rho_{hw} u_{hw} d_i}{\mu_{hw}} = \frac{4G_{hw}}{\pi d_i \mu_{hw}}, \tag{6}$$

where ρ_{hw}, u_{hw} and μ_{hw} are the density, velocity and dynamic viscosity, respectively, of the superheated water exiting the inner tube at $z = 0$ and d_i is the inside diameter of the inner tube. It is assumed the viscous drag force does not change appreciably as the superheated water exits the inner tube into the opposing flow of the combined mixture (however this may not be the case, particularly if the combined mixture is near-critical with a correspondingly low viscosity). The relative magnitude of the momentum of the jet acting downwards compared to the buoyancy force acting upwards (owing to the differences in density between the superheated water and the cooler mixture around it) can be represented [27] by the square of the Froude number $(Fr_{hw,z=0})^2$ (equal to the reciprocal of the Richardson number, Ri):

$$(Fr_{hw,z=0})^2 = Ri^{-1} = \frac{\rho_{hw} {u_{hw}}^2}{d_i(\rho_m - \rho_{hw})g} = \frac{16{G_{hw}}^2}{\pi^2 {d_i}^5 \rho_{hw}(\rho_m - \rho_{hw})g}, \tag{7}$$

where ρ_m is the density of the mixture determined from the temperature measured at $z = 0$. When $(Fr_{hw,z=0})^2$ is greater than 1 the momentum of the jet dominates, pushing the superheated water further into the oncoming flow of 'precursors', whilst a magnitude of $(Fr_{hw,z=0})^2$ much less than unity suggests buoyancy forces dominate, causing a more rapid reversal in the direction of the jet of superheated water towards the outlet of the mixer. Table 1 gives the magnitudes of $Re_{hw,z=0}$ and $(Fr_{hw,z=0})^2$ for all the experiments; the transport properties for the mixtures were determined at the measured 30-s average temperature of the mixture at $z = 0$ and for the superheated water at $T'_{hw,z=0}$, determined from Eqs. (2) and (3). Attention is drawn to the wide variation in the density and dynamic viscosity of the jet of superheated water exiting the inner pipe at $z = 0$, *e.g.* between experiment no. 2 in Table 1 (density of the superheated water $\rho_{hw} = 732\ kg\,m^{-3}$ and viscosity, $\mu_{hw} = 9.0 \times 10^{-5}$ Pa s) and experiment no. 9 ($\rho_{hw} = 161\ kg\,m^{-3}$ and $\mu_{hw} = 2.9 \times 10^{-5}$ Pa s). As a result, the velocity of the superheated water, u_{hw} at position $z = 0$ increased from 0.2 to 1.1 $m\,s^{-1}$, due to thermal expansion alone, since the mass flowrate of the superheated water was the same in both experiments.

The magnitude of $Re_{hw,z=0}$ in Table 1 indicate that the flow of superheated water may be laminar ($Re_{hw} < 2300$) or turbulent depending on the flowrates and temperatures used. In particular, the jet appears to be turbulent ($Re_{hw,z=0} \approx 1 \times 10^4$) in the experiments using unbalanced flows and $T_{hw,in} \geq 400$ °C. Expressed in terms of the mass flowrate of superheated water, G_{hw}, it is clear from Eq. (6) that $Re_{hw,z=0}$ depends only on dynamic viscosity, μ_{hw}, for a given inside diameter of the inner tube, d_i, and G_{hw} and thus, this increase in $Re_{hw,z=0}$ is due to the lower viscosity of the superheated water.

The magnitudes of $(Fr_{hw,z=0})^2$ given in Table 1 for the experiments at the lowest, but balanced, flowrates, suggest that the momentum of the jet and the buoyancy force opposing it are of a similar magnitude, *i.e.* $(Fr_{hw,z=0})^2 \approx 1$. At the higher balanced flowrates, momentum begins to dominate over the buoyancy force, *i.e.* $(Fr_{hw,z=0})^2 > 1$. For the experiments in which the flowrates were unbalanced, the magnitude of $(Fr_{hw,z=0})^2$ increased from 11.5 at $T_{hw,in} = 350$ °C to 21.8 at 400 °C and 44.9 at 450 °C. Since $(Fr_{hw,z=0})^2 \gg 1$ (particularly when $T_{hw,in} > 400$ °C) the superheated water exits the inner pipe as a 'turbulent jet'. This has implications for scaling-up the counter-current mixer; for example, should one wish to scale-up G_{hw} by a factor of 100, d_i must be increased by a factor of 6.3 to keep $(Fr_{hw,z=0})^2$ constant between the scales,

thus, ensuring the relative magnitude of the momentum and buoyancy forces remain the same on the larger scale. However, in doing so $Re_{hw,z=0}$ will increase by a factor of ~16, which may result in a transition from a laminar flow of superheated water to a turbulent one.

The undesirable penetration of the jet of superheated water deep into the precursor when the flowrates are unbalanced and at $T_{hw,in} \geq 400\,^{\circ}C$, evident in the temperature measurements shown in Figs. 3 and 5, appears to result from two factors: (i) a transition from a situation in which the momentum of the jet of superheated water is approximately in balance with the drag and buoyancy forces opposing it ($Re_{hw,z=0} \approx 2000$ and $(Fr_{hw,z=0})^2 \approx 1$) to one in which momentum dominates ($Re_{hw,z=0} \approx 10{,}000$ and $(Fr_{hw,z=0})^2 \gg 1$) and (ii) the effect of thermal dilation, due to entrainment of the mixture of 'precursors' and superheated water into the jet of superheated water issuing from the inner pipe, is less significant when the mixture is above the critical temperature of water (low density) than when it is below the critical temperature (much higher density).

4. Conclusions

Processes of mixing and heat transfer inside a counter-current mixer, of a design previously used for the continuous hydrothermal synthesis of a range of different inorganic nanoparticles, have been studied by measuring temperatures in situ at typical operating conditions. Thus, this work has better defined the conditions for the synthesis, in a counter-current mixer, of many different types nanoparticles.

For balanced flowrates (when the flowrates of the superheated water and 'precursors' were equal on a mass basis), the superheated water issuing from the inner pipe did not penetrate far into the 'precursors'. However, large, rapid fluctuations in temperature with time were observed below the outlet of the inner pipe when the flows were unbalanced (an excess of superheated water) and $T_{hw,in}$ was greater than or equal to 400 °C. This suggests that under these conditions a jet of supercritical water penetrated into the 'precursors'. Such jetting may be considered undesirable for the controlled synthesis of nanoparticles.

An increase in temperature of the products as they flowed up through the annulus between the inner and outer pipes was measured. This was the result of the internal transfer of heat between the superheated water and the cooler products. Consequently, the temperature in the region where the superheated water and 'precursors' meet, *i.e.* the point at which nanoparticles begin to form, was substantially lower than that predicted by an overall heat balance on the mixer. This maximum theoretical temperature was approached only at the outlet of the mixer.

The balance of forces (momentum, drag and buoyancy) acting on the jet of superheated water, just as it emerged from the inner pipe, was quantified by determining the Reynolds and Froude numbers at the outlet, $Re_{hw,z=0}$ and $(Fr_{hw,z=0})^2$, respectively. As $T_{hw,in}$ was increased, $Re_{hw,z=0}$ increased owing to the decrease in the viscosity of water with temperature. At the same time $(Fr_{hw,z=0})^2$ increased, indicating that the downwards momentum of the jet began to overcome the opposing buoyancy force. At the conditions which resulted in large, rapid fluctuations in temperature below the outlet of the inner tube, the jet of superheated water was both turbulent ($Re_{hw,z=0} \approx 1 \times 10^4$) and momentum-dominated, *i.e.* $(Fr_{hw,z=0})^2 \gg 1$.

The authors have employed the experimental methods described in this work in the assessment of alternative designs of mixer for the CHFS process, *e.g.* a co-current 'confined jet' mixer. Experiments and CFD simulations to investigate transport processes within this new mixer will be reported in due course.

Acknowledgements

The EPSRC are thanked for funding the project "Continuous Hydrothermal Synthesis of Nanoparticles: From Laboratory to Pilot Plant" (reference no. EP/E040551/1 for C.J.T., R.G. and J.A.D., and EP/E040624/1 for C.Y.M., T.M. and X.Z.W.).

References

[1] T. Adschiri, K. Kanazawa, K. Arai, Rapid and continuous hydrothermal crystallization of metal-oxide particles in supercritical water, Journal of the American Ceramic Society 75 (1992) 1019–1022.
[2] A. Cabanas, J.A. Darr, E. Lester, M. Poliakoff, A continuous and clean one-step synthesis of nano-particulate $Ce_{1-x}Zr_xO_2$ solid solutions in near-critical water, Chemical Communications (2000) 901–902.
[3] A. Cabanas, J.A. Darr, E. Lester, M. Poliakoff, Continuous hydrothermal synthesis of inorganic materials in a near-critical water flow reactor; the one-step synthesis of nano-particulate $Ce_{1-x}Zr_xO_2$ ($x = 0$–1) solid solutions, Journal of Materials Chemistry 11 (2001) 561–568.
[4] X.L. Weng, J.Y. Zhang, Z.B. Wu, Y. Liu, H.Q. Wang, J.A. Darr, Continuous hydrothermal syntheses of highly active composite nanocatalysts, Green Chemistry 13 (2011) 850–853.
[5] Z.C. Zhang, S. Brown, J.B.M. Goodall, X.L. Weng, K. Thompson, K.N. Gong, S. Kellici, R.J.H. Clark, J.R.G. Evans, J.A. Darr, Direct continuous hydrothermal synthesis of high surface area nanosized titania, Journal of Alloys and Compounds 476 (2009) 451–456.
[6] A.A. Chaudhry, S. Haque, S. Kellici, P. Boldrin, I. Rehman, A.K. Fazal, J.A. Darr, Instant nano-hydroxyapatite: a continuous and rapid hydrothermal synthesis, Chemical Communications (2006) 2286–2288.
[7] X.L. Weng, D. Brett, V. Yufit, P. Shearing, N. Brandon, M. Reece, H.X. Yan, C. Tighe, J.A. Darr, Highly conductive low nickel content nano-composite dense cermets from nano-powders made via a continuous hydrothermal synthesis route, Solid State Ionics 181 (2010) 827–834.
[8] E. Lester, P. Blood, J. Denyer, D. Giddings, B. Azzopardi, M. Poliakoff, Reaction engineering: the supercritical water hydrothermal synthesis of nano-particles, Journal of Supercritical Fluids 37 (2006) 209–214.
[9] A. Aimable, H. Muhr, C. Gentric, F. Bernard, F. Le Cras, D. Aymes, Continuous hydrothermal synthesis of inorganic nanopowders in supercritical water: towards a better control of the process, Powder Technology 190 (2009) 99–106.
[10] Y. Wakashima, A. Suzuki, S. Kawasaki, K. Matsui, Y. Hakuta, Development of a new swirling micro mixer for continuous hydrothermal synthesis of nano-size particles, Journal of Chemical Engineering of Japan 40 (2007) 622–629.
[11] R. Gruar, C.J. Tighe, L.M. Reilly, G. Sankar, J.A. Darr, Tunable and rapid crystallisation of phase pure Bi_2MoO_6 (koechlinite) and $Bi_2Mo_3O_{12}$ via continuous hydrothermal synthesis, Solid State Sciences 12 (2010) 1683–1686.
[12] E.J. List, Turbulent jets and plumes, Annual Review of Fluid Mechanics 14 (1982) 189–212.
[13] K.G. Bemis, R.P. Vonherzen, M.J. Mottl, Geothermal heat-flux from hydrothermal plumes on the Juan-de-Fuca ridge, Journal of Geophysical Research-Solid Earth 98 (1993) 6351–6365.
[14] C.Y. Ma, C.J. Tighe, R.I. Gruar, T. Mahmud, J.A. Darr, X.Z. Wang, Numerical modelling of hydrothermal fluid flow and heat transfer in a tubular heat exchanger under near critical conditions, Journal of Supercritical Fluids 57 (2011) 236–246.
[15] V. Middelkoop, P. Boldrin, M. Peel, T. Buslaps, P. Barnes, J.A. Darr, S.D.M. Jacques, Imaging the inside of a continuous nanoceramic synthesizer under supercritical water conditions using high-energy synchrotron X-radiation, Chemistry of Materials 21 (2009) 2430–2435.
[16] T. Rothenfluh, M.J. Schuler, P.R. von Rohr, Penetration length studies of supercritical water jets submerged in a subcritical water environment using a novel optical Schlieren method, Journal of Supercritical Fluids 57 (2011) 175–182.
[17] C.Y. Ma, C.J. Tighe, R.I. Gruar, T. Mahmud, J.A. Darr, X.Z. Wang, Numerical simulation of fluid flow and heat transfer in a counter-current reactor system for nanomaterial production, Chemical Product and Process Modelling 6 (2011), Article 6.
[18] J. Sierra-Pallares, D.L. Marchisio, E. Alonso, M. Teresa Parra-Santos, F. Castro, M. Jose Cocero, Quantification of mixing efficiency in turbulent supercritical water hydrothermal reactors, Chemical Engineering Science 66 (2011) 1576–1589.
[19] L.L. Toft, D.F. Aarup, M. Bremholm, P. Hald, B.B. Iversen, Comparison of T-piece and concentric mixing systems for continuous flow synthesis of anatase nanoparticles in supercritical isopropanol/water, Journal of Solid State Chemistry 182 (2009) 491–495.
[20] P. Boldrin, A.K. Hebb, A.A. Chaudhry, L. Otley, B. Thiebaut, P. Bishop, J.A. Darr, Direct synthesis of nanosized $NiCo_2O_4$ spinel and related compounds via continuous hydrothermal synthesis methods, Industrial and Engineering Chemistry Research 46 (2007) 4830–4838.
[21] A.A. Chaudhry, H.X. Yan, K.N. Gong, F. Inam, G. Viola, M.J. Reece, J.B.M. Goodall, I.U. Rehman, F.K. McNeil-Watson, J.C.W. Corbett, J.C. Knowles, J.A. Darr, High-strength nanograined and translucent hydroxyapatite monoliths via continuous hydrothermal synthesis and optimized spark plasma sintering, Acta Biomaterialia 7 (2011) 791–799.
[22] S. Kellici, K.A. Gong, T.A. Lin, S. Brown, R.J.H. Clark, M. Vickers, J.K. Cockcroft, V. Middelkoop, P. Barnes, J.M. Perkins, C.J. Tighe, J.A. Darr, High-throughput

continuous hydrothermal flow synthesis of Zn–Ce oxides: unprecedented solubility of Zn in the nanoparticle fluorite lattice, Philosophical Transactions of the Royal Society A: Mathematical Physical and Engineering Sciences 368 (2010) 4331–4349.
[23] A.A. Chaudhry, J. Goodall, M. Vickers, J.K. Cockcroft, I. Rehman, J.C. Knowles, J.A. Darr, Synthesis and characterisation of magnesium substituted calcium phosphate bioceramic nanoparticles made via continuous hydrothermal flow synthesis, Journal of Materials Chemistry 18 (2008) 5900–5908.
[24] W. Wagner, A. Pruss, The IAPWS formulation 1995 for the thermodynamic properties of ordinary water substance for general and scientific use, Journal of Physical and Chemical Reference Data 31 (2002) 387–535.
[25] J.M. Coulson, J.F. Richardson, J.R. Backhurst, J.H. Harker, Chemical Engineering, vol. 1, 6th ed., Butterworth-Heinemann, Oxford, 1999.
[26] H.S. Swenson, J.R. Carver, C.R. Kakarala, Heat transfer to supercritical water in smooth-bore tubes, Journal of Heat Transfer 87 (1965) 477–483.
[27] W. Rodi (Ed.), Turbulent Buoyant Jets and Plumes, Pergamon Press, Oxford, 1982.